Journal Pre-proofs

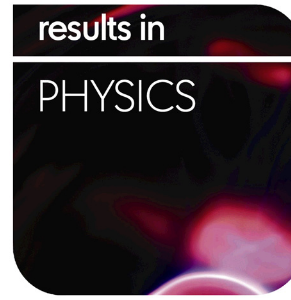

Electrical properties of La^{3+} and Y^{3+} ions substituted $Ni_{0.3}Cu_{0.3}Zn_{0.4}Fe_2O_4$ nano-spinel ferrites

M. Almessiere, B. Ünal, Y. Slimani, A.D. Korkmaz, A. Baykal, I. Ercan

PII: S2211-3797(19)32630-0
DOI: https://doi.org/10.1016/j.rinp.2019.102755
Reference: RINP 102755

To appear in: *Results in Physics*

Received Date: 30 August 2019
Revised Date: 18 September 2019
Accepted Date: 14 October 2019

Please cite this article as: Almessiere, M., Ünal, B., Slimani, Y., Korkmaz, A.D., Baykal, A., Ercan, I., Electrical properties of La^{3+} and Y^{3+} ions substituted $Ni_{0.3}Cu_{0.3}Zn_{0.4}Fe_2O_4$ nanospinel ferrites, *Results in Physics* (2019), doi: https://doi.org/10.1016/j.rinp.2019.102755

Electrical properties of La^{3+} and Y^{3+} ions substituted $Ni_{0.3}Cu_{0.3}Zn_{0.4}Fe_2O_4$ nanospinel ferrites

M. Almessiere[a,b,1], B. Ünal[c], Y. Slimani[a], A.D. Korkmaz[d], A. Baykal[e], I. Ercan[a]

[a]Department of Biophysics, Institute for Research & Medical Consultations (IRMC), Imam Abdulrahman Bin Faisal University, P.O. Box 1982, 31441, Dammam, Saudi Arabia.

[b]Department of Physics, College of Science, Imam Abdulrahman Bin Faisal University, P.O. Box 1982, 31441, Dammam, Saudi Arabia.

[c]Institute of Forensic Sciences & Legal Medicine, **and Institute of Nanotechnology & Biotechnology,** Istanbul University - Cerrahpaşa, Buyukcekmece Campus, Alkent 2000 Mah., Buyukcekmece-Istanbul 34500, Turkey.

[d]Department of Chemistry, Istanbul Medeniyet University, 34700 Istanbul, Uskudar, Turkey.

[e]Department of Nano-Medicine Research, Institute for Research & Medical Consultations (IRMC), Imam Abdulrahman Bin Faisal University, P.O. Box 1982, 31441, Dammam, Saudi Arabia.

Abstract

La–Y substituted Ni-Cu-Zn nanospinel ferrites (NSFs) having the following formula $Ni_{0.3}Cu_{0.3}Zn_{0.4}La_xY_xFe_{2-2x}O_4$ (x=0.0 - 0.10) were fabricated prepared by ultrasonic irradiation approach. The X-ray powder diffractometer (XRD), scanning electron microscope (SEM) and Fourier-transform infrared spectroscopy (FT-IR) were utilized to analyze the structure, vibration bands and morophology. The impedance spectrocopy technique was used for the analysis of electrical and dielectric properties of La^{3+} and Y^{3+} ions co-substituted $Ni_{0.3}Cu_{0.3}Zn_{0.4}Fe_2O_4$ NSFs. Some important parameters such as ac conductivity, activation

[1] **Corresponding Author: Email:** malmessiere@iau.edu.sa (M.A. Almessiere).

energy, dielectric constant and dielectric loss were examined as functions of frequencies and temperatures for a variety of La and Y co-substitution ratios. **In general, ac conductivity is observed to fluctuate slightly with the elevated temperatures while its fluctuation level decreases somehow with an increase in co-substitution ratios. Furthermore, the** frequency dependence of dielectric functions **could be** described by Koop's models based on Maxwell-Wagner theory, which elucidates the correlation between the polarizability coefficient and dielectric constant in inhomogeneous double-layer structures.

Keywords: Spinel ferrites; Rare earth substitutions; Conductivity; Dielectric properties.

1. Introduction

During last years, there has been a major effort to design, prepare, characterize, and use novel materials for different applications. Nano-sized spinel ferrites (NSFs) are soft ferrites, a class of magnetic nanoparticles (MNPs), which have been a target of many research studies due to their optimum magnetic, dielectric, optical, and catalytic properties which differ from their bulk counterparts [1]. Advances in the research and development lead to use soft ferrites in many fields including health such as biomedical imaging, hyperthermia, drug delivery, energy such as gas sensors, catalysis and bioremediation, and technology such as super-capacitors, nonvolatile memory devices, on-chip inductors, and microwave absorbers [2-7]. NSFs have the spinel structure with a formula AFe_2O_4 wherein A is a divalent metal ion in T_d sites and Fe^{3+} is in O_h sites for normal spinel ferrites. In the crystal structure of NSFs, there are intra-sublattice (A-O-A and A-O-B) and inter-sublattice (A-O-B) super-exchange interactions with inter-sublattice interactions being much stronger than the intra-interactions and responsible for ferrimagnetic ordering [8, 9]. Hence, if the ferric ion in the octahedral site is substituted by a nonmagnetic ion, B-B interactions will be decreased and consecutively A-B interactions and the overall magnetization and *vice versa*.

Nickel copper zinc ferrite is a spinel ferrite which mainly is used as multilayer chip inductors in various devices such as mobile phones and laptop computers. NiCuZn ferrites have been known with high resistivity in the high-frequency field and high saturation magnetization. However, for further miniaturization of communication devices, it is essential to develop the magnetic and dielectric properties of NiCuZn ferrites. Therefore, many attempts to replace the cations in the crystal structure of NiCuZn ferrites have been made in order to obtain novel materials with improved performance. For example, a study by Roy and Bera showed that Mg^{2+} substitution enhanced the *ac* resistivity and the permeability in addition to lowering the magnetic loss of the sol-gel auto combustion synthesized $Ni_{0.25}Cu_{0.20}Zn_{0.55})Fe_2O_4$ ferrite [10]. Rashid et al. explored how Sc^{3+} doping affected magnetic and dielectric behavior of NiCuZn ferrites ($Ni_{0.3}Cu_{0.2}Zn_{0.5}Sc_xFe_{2-x}O_4$). The substitution of NiCuZn ferrites with Sc^{3+} resulted in an initial drop in the real part of permittivity at low-frequency region (<10^5 kHz) but almost no change in the high frequency region (>10^5 kHz) with increasing frequency; which were found to obey Maxwell-Wagner model. The initial permeability dropped till x=0.02, rose till x=0.05 and finally dropped again when x=0.07 with increasing frequency, at low-frequency region. At high-frequency area, both parts of the initial permeability remained constant with increasing Sc^{3+} concentration but dropped in general which was explained by pores within the grains and magnetic impurities among grains hindering domain walls and spin motions. The authors observed a variation in the *ac* resistivity with different frequencies in a similar trend to that of the permeability. This was explained by the electron hoping behavior among Fe^{3+} and Fe^{2+} ions. At high substitution ratios, the preference of B-sites by the dopant ions caused a rise in the resistivity and a decrease in the saturation magnetization [11]. Eltabey et al. examined the consequence of introducing aluminum ions to NiCuZn ferrites ($Ni_{0.4}Cu_{0.2}Zn_{0.4}Al_xFe_{2-x}O_4$) synthesized by the ceramic method. The rise in the aluminum concentration increased the crystallite size, enhanced the initial permeability, magnetization, and the *dc* resistivity while no significant influence was observed for Curie temperature [12].

Rare earth (RE) metals have been used in many technological applications including telecommunication. Scientists have been studying the influence of incorporation of RE ions in electromagnetic and optical properties of NiCuZn ferrites as well as other NSFs. Chaudhari and co-workers investigated the effect of lanthanum doping in NiCuZn NSFs ($Ni_{0.5}Cu_{0.25}Zn_{0.25}La_xFe_{2-x}O_4$, where $x \leq 0.1$) fabricated by sol-gel technique [13]. The substitution of Fe^{3+} ion with La^{3+} ion resulted in an increased *dc* resistivity as well as elevated activation energy (E_a) due to structural disorder brought by the increasing amount of the lanthanum ion. They also obtained a decreased saturation magnetization (Ms) with increasing La^{3+} substitution owing to the nonmagnetic nature of lanthanum. The averaged crystallites size of the particles has also a big impact on the saturation magnetization. For instance, in a study, $Ni_{0.4}Cu_{0.2}Fe_{1.95}RE_{0.05}O_4$ nanoparticles doped with rare earth ions by an ultrasound irradiation-assisted co-precipitation displayed a decreasing crystallite size with Pr^{3+}, Sm^{3+}, Eu^{3+}, and Sm^{3+} doped NiCuZn ferrites and also decreasing Ms values with respective crystallite sizes obtained from XRD analyses [14]. In conclusion, the substitution of cations in NiCuZn ferrites may improve their dielectric and magnetic characteristics. However, we were not able to find any studies on the influence of co-substitutions of La^{3+} and Y^{3+} on NiCuZn NSFs.

In this study, the synthesis and characterization of double-substituted $Ni_{0.4}Cu_{0.2}Zn_{0.4}La_xY_xFe_{2-x}O_4$ (x=0.00 - 0.10) NSFs produced by ultrasonic irradiation method were presented. The structure, morphology, spectral, electrical and dielectric properties were reported.

2. Experimental details

$Ni_{0.3}Cu_{0.3}Zn_{0.4}La_xY_xFe_{2-2x}O_4$ (x=0.0 - 0.10) NSFs were prepared with Ultrasonic irradiation process. $Zn(NO_3)_2{\cdot}6H_2O$, $Cu(NO_3)_2{\cdot}3H_2O$, $Ni(NO_3)_2{\cdot}6H_2O$, $La(NO_3)_3.6H_2O$, $Fe(NO_3)_3{\cdot}9H_2O$, $C_6H_8O_7$ and Y_2O_3, are all analytical grade (sigma Aldrich) and were utilized as started materials. Initially, Y_2O_3 was thawed in 10 ml of conc. HCl at 150 °C until the solution became transparent. The metals salts with citric acid are thawed in 80 ml of DI water then added on Y_2O_3 solution under stirring. The Ultrasonic irradiation procedure was described in our earlier publication [15,16].

The structure analysis has been done through Rigaku Benchtop Miniflex X-ray diffraction (XRD) with CuKα radiations. The morphology, size and chemical compositions were performed using FEI Teneo scanning electron microscope (SEM) equipped with an EDX detector. Bruker Fourier-transform infrared (FT-IR) spectrophotometer was used for the spectral analysis (4000 to 400 cm^{-1}). **All the samples were prepared in pellets and the dielectric measurements were performed using double parallel electrodes such as sandwich form via Novocontrol Alpha-N high-resolution impedance analyzer.**

3. Results and discussion

3.1. Structure

XRD patterns of $Ni_{0.4}Cu_{0.2}Zn_{0.4}La_xY_xFe_{2-x}O_4$ (x=0.00-0.10) NSFs were presented in Figure 1. The phase identification was confirmed the single-phase formation of NiCuZn without of any impurity. The full proof software was used in order to do Rietveld refinement for calculating the lattice parameters (Table 1). Debye–Scherrer equation was used to calculate the average crystallites size (Table 1). The lattice parameter ‘a’ increases with adding La-Y as a result of the distortion of the crystal structure initiated from the occupation of octahedral sites by large ionic radii of La^{3+} and Y^{3+} substitution ions. The average crystallites size slightly decreases from about 23 to 12 nm with the increase of La-Y concentration.

Figure 1.

Table 1.

3.2. Microstructural analysis

The FE-SEM images of $Ni_{0.4}Cu_{0.2}Zn_{0.4}La_xY_xFe_{2-x}O_4$ (x=0.00, 0.02, 0.06 and 0.10) NSFs were shown in Figure 2. The images exhibited smaller spherical grains with size in the range of few tens nanometer. These grains are aggregated as a result of the magnetic interactions. EDX and elemental mapping of $Ni_{0.4}Cu_{0.2}Zn_{0.4}La_xY_xFe_{2-x}O_4$ (x=0.04 and 0.08) (Figure 3) disclosed a homogeneous chemical composition with presence of different elements of Zn, Fe, La, Ni, Y, Cu and O which verified the creation of the desired compositions.

Figure 2.

Figure 3.

3.3. FT-IR

FT-IR spectra of $Ni_{0.4}Cu_{0.2}Zn_{0.4}La_xY_xFe_{2-x}O_4$ (x=0.00-0.10) NSFs were presented in Figure 4. The highest one, ν_1, generally observed in the range 554 cm^{-1}, corresponds to intrinsic stretching vibrations of the metal at the tetrahedral site, $M_{tetra} \leftrightarrow O$, whereas the ν_2-lowest band, usually observed in the range 403 cm^{-1}, is assigned to octahedral metal stretching, $M_{octa} \leftrightarrow O$ [17]. It is clearly that the changing in position of 554 cm^{-1} band was due to the distributions of substituted ions at the lattice sites which caused a variation in the length of iron oxygen bond [18]. These changing is a result of inverse spinel structure of $NiFe_2O_4$, So there is possibility that the substituted ions can move between A and B-site.

Figure 4.

3.4. Electrical and dielectric properties

Any spinel ferrite nanostructure plays some important role in many technological usages such as microwave, hyperthermia, nonvolatile memory device and super capacitor applications [19-

21]. So, the complex impedance analysis has a powerful characterization techniques to evaluate the electrical properties of many ferrite nanomaterials. Each of the parameters relative to the dielectric and electrical properties is also important to examine the characteristics of spinel structure. These characteristic parameters realize some contributions based on the grains size effect and interfacial properties amongst grains boundaries, which comprises a diversity of properties for example dielectric constant, conductivity, temperature and loss as a function of frequency as well as various single or multiple substitutions of many types. The fundamental characteristics of conductivity can be originated from two parts; these are the *dc* conductivity on account of band conduction mechanism and the *ac* conductivity due to hopping conduction mechanisms resulting in the charge carriers being transported between identical ions of any given elements occurring in numerous valence states. This could be attributed to a tendency of the power law dependency. Therefore, the characterization of ac conductivity of $Ni_{0.4}Cu_{0.2}Zn_{0.4}La_xY_xFe_{2-x}O_4$ (x=0.00-0.10) NSFs for the La and Y ions substitutions between x=0.00 to 0.10 have been investigated extensively under a 3D plot formalism.

All the graphs given in Figure 5 that ac conductivities indicate an almost linear tendency in the natural *logσ-logf* plots for any linearly elevated temperature while less influence is observed for temperatures up to 120°C. This reveals that conductivity follows a power law against frequency as follows:

$$\sigma(\omega,T,x) = \sigma(T,x)\omega^n$$

where, the exponent '*n*' varies marginally with various La and Y ions co-substitutional ratios but leads to a variety of dependencies over a certain temperature range. The x=0.02 graph of the 3D semi-*lnσ-lnf-T* formalism in Figure 5 shows that the conductivity at lower frequencies possesses more influence compared to other co-substitutional ratios including the unsubstituted sample, but signifies that a sharp escalation in conduction mechanism is recorded over a high frequency region for x=0.06. Additionally, any conductivity at high frequencies causes a sharp drop for certain co-substitution ratios of x=0.06-0.10 of La and Y ions in $Ni_{0.3}Cu_{0.3}Zn_{0.4}$:Fe_2O_4

NSFs. In general, ac conductivity is observed to fluctuate slightly with the elevated temperatures; however, fluctuation level decreases somehow with an increase in co-substitution ratios. This fluctuation reveals an increase in conductivity with the elevated temperature. This fluctuation is more common in high temperature conductivity for the co-substitutional ratios of x=0.06-0.10.

Figure 5.

Arrhenius plot of dc conductivity for various co-substitutions of La and Y ions in $Ni_{0.3}Cu_{0.3}Zn_{0.4}Fe_2O_4$ NSFs is shown in Figure 6. Each curve illustrates several trends in activation energy according to the temperature variations between 20 ^oC and 120 ^oC. Any substitutional ratios of La and Y ions in $Ni_{0.3}Cu_{0.3}Zn_{0.4}Fe_2O_4$ NSFs have more effects on the variations of activation energy and gives a variety of tendencies along co-substitutional ratios. Furthermore, dc conductivity increases with the ion-exchange of co-substitutions in $Ni_{0.3}Cu_{0.3}Zn_{0.4}Fe_2O_4$ NSFs. The dc conductivity gives us a different trend over 350K while it becomes less variation under 350K except for high co-substitution ratios. Maximum conductivity variation is observed for the sample of x=0.02 while for unsubstituted one there exists no activation energy recorded a temperature below 340K. As activation energies for all the NSFs could take both signed values (because of fluctuation) along the studied temperature range, only regular variation is observed for the sample of x=0.06. This means that co-substitutions can be used for controlling the conduction mechanism of the NSFs.

The conduction mechanism could also be interpreted as follows; one contribution can possibly be considered as the charge carriers in nanocrystallites spinel ferrites (NCSFs) due to O2p holes (or O2p electrons) [22-24]. Another option can be due to the interfaces between the grains and grain boundries for either polycrystallites or NCSFs, having an important effect on the fluctuation of conduction mechanism as mentioned earlier. [25].

Figure 6.

The 3D characterizations of dielectric constant of $Ni_{0.4}Cu_{0.2}Zn_{0.4}La_xY_xFe_{2-x}O_4$ (x=0.00-0.10) NSFs is shown in Figure 7 for La^{3+} and Y^{3+} ions co-substitutional ratios ranging ($0.00 \leq x \leq 0.10$). At lower frequencies, any dielectric constant for each ratio of La and Y ion-substitutions changes with a variety of tendencies at the elevated temperature while some type of consistencies is elucidated in the moderate and higher frequency ranges as a function of temperature. This means that any level of substitution presents a significant influence on dielectric constant, especially in low frequency interval. This tendency could sometimes be a fluctuation, and a decrease or an increase. In all cases, the dielectric constant reduces with rising frequency. It can also be noted that any co-substitution ratio results in a rise in dielectric constant when compared with unsubstituted sample. These trends are mostly consistent with any substituted spinel ferrites [26, 27].

Figure 7.

The 3D characteristic tendencies of dielectric loss of $Ni_{0.4}Cu_{0.2}Zn_{0.4}La_xY_xFe_{2-x}O_4$ (x=0.00-0.10) NSFs spinel ferrites are shown in Figure 8 for a variety of La^{3+} and Y^{3+} ion co-substitutions ranging from x=0.00 to 0.10. Dielectric loss increases slightly with the elevated temperature at low frequencies for some low co-substitutional ratios such as x=0.02, 0.04 and 0.06. However, for the high co-substitutional ratios it fluctuates at lower frequencies. In all co-substituted cases, dielectric loss decreases with increasing frequency, while temperature change has a significant effect at higher frequencies for all substitution levels. The dielectric loss of unsubstituted ferrites is both low and the deep variability is different from others, some of which are similar to x = 0.06.

Figure 8.

The dielectric tangent loss, also known as dissipation factor, of $Ni_{0.4}Cu_{0.2}Zn_{0.4}La_xY_xFe_{2-x}O_4$ (x=0.00-0.10) NSFs is presented in Figure 9 for a variety of La^{3+} and Y^{3+} ions co-substitutional ratios between x=0.00 and 0.10 in the 3D plot representation. The dissipation factor gives us a maximum peak at low frequency for high temperature for substitution x = 0.02, but the other substitution provides a peak for similar conditions. The tangential loss factor drops suddenly for substitution ratios of 0.02, 0.04 and 0.06, but decreases with increasing frequency and decreasing temperatures in all cases. Furthermore, for high x = 0.08 and 0.10 substituted samples, the loss factor first increases and then decreases and finally offers a peak at high temperature in the low frequency range. For the unsubstituted reference sample, the characteristic dispersion factor first shrinks, then falls down to a minimum value, and then increases with increasing frequency. Thus, temperature dependence at low frequency is more effective.

Figure 9.

In general, the dielectric constant of $Ni_{0.4}Cu_{0.2}Zn_{0.4}La_xY_xFe_{2-x}O_4$ (x=0.00-0.10) NSFs decreases in a fairly regular trend with rising frequency, and the reduction rate is almost similar for various products. This relative variation indicates the existence of electrode interface polarization processes that occur at low frequencies [28]. Curve trends are maintained almost unchanged. Thus, the dielectric constant decreases sharply depending on how fast polarization occurs to continue with the oscillations of the electric fields. If the frequency is increased, the orientation polarization decreases as the alignment of the dipole moments leads to lessening the dielectric constant and therefore requires longer time than ionic and electronic polarizations. The frequency dependence of dielectric functions could be explained by Koop's models based on Maxwell-Wagner theory that clarify the relationship between the dielectric constant and the polarizability coefficient in inhomogeneous double-layer structures [29, 30]. The effective layer that contributes to the conductivity is large ferrite grains separated by moderately weak conductive grain boundaries [31]. While grain boundaries are seen to be efficient at low frequencies, grains dominate at higher frequencies as seen from the dielectric distribution curves studied here [32, 33]. Particularly in the case of temperature dependence at low frequency range, the dielectric constant is slightly increased due to molecular orientation and arrangement [34]. Therefore, at low frequencies, polarization at the grain boundaries requires high energies, causes high energy loss, and polarization in grains requires low energy, and therefore causes low energy losses at high frequency range [35, 36]. The interface polarization occurs at lower frequencies however other polarization mechanisms like electronic and ionic are introduced at high frequency range [37-39]. Dielectric loss, therefore, turns out to be high dependencies in frequency, and somewhat less sensitive to temperature so the variation is rather high at high frequency regime for a variety of co-substitution ratios.

4. Conclusion

$Ni_{0.4}Cu_{0.2}Zn_{0.4}La_xY_xFe_{2-x}O_4$ (x=0.00-0.10) NSFs were synthesized by exposing it to ultrasonic irradiation. The construction of spinel ferrite was approved by XRD, SEM and FT-IR. It is found that with rising the content of La-Y**, the lattice constants growth due to** the **expansion** of crystal. Electrical and dielectric properties shows that **(i)** ac conductivity obeys the power exponent rules, and **the better consistency in conduction mechanism were obtained from the co-substitution of x=0.04,** **(ii)** the activation energies for the $Ni_{0.3}Cu_{0.3}Zn_{0.4}Fe_2O_4$ NPs fluctuate with the co-substitution ratios of La^{3+} and Y^{3+} ions; **(iii)** both dielectric loss and dielectric constant decrease sharply with increasing frequencies under a power law formalism. The frequency dependence of dielectric functions is enlightened by Koop's models based on Maxwell-Wagner theory.

References

[1] D. El Kony, S.A. Saafan, Dielectric Properties and Magnetic Susceptibility of Mn-Zn Ferrites/SiO_2 Composites, Journal of American Science, 8 (2012) 51-57.

[2] N. Sanpo, C.C. Berndt, C. Wen, J. Wang, Transition metal-substituted cobalt ferrite nanoparticles for biomedical applications, Acta Biomaterialia, 9 (2013) 5830-5837.

[3] M.D. Shultz, S. Calvin, P.P. Fatouros, S.A. Morrison, E.E. Carpenter, Enhanced ferrite nanoparticles as MRI contrast agents, Journal of Magnetism and Magnetic Materials, 311 (2007) 464-468.

[4] A. Hanini, L. Lartigue, J. Gavard, K. Kacem, C. Wilhelm, F. Gazeau, F. Chau, S. Ammar, Zinc substituted ferrite nanoparticles with $Zn_{0.9}Fe_{2.1}O_4$ formula used as heating agents for in vitro hyperthermia assay on glioma cells, Journal of Magnetism and Magnetic Materials, 416 (2016) 315-320.

[5] S.V. Jagtap, A.V. Kadu, N.N. Gedam, G.N. Chaudhari, Ammonia Gas Sensing Properties of Nanocrystalline $Zn_{1-x}Cu_xFe_2O_4$ Doped with Noble Metal, Sensors & Transducers Journal, 122 (2010) 120-127.

[6] F. Liu, T. Ren, C. Yang, L. Liu, A.i. Wang, J. Yu, NiCuZn ferrite thin films for RF integrated inductors, Mater. Lett. 60(2006) 1403-1406.

[7] M. Pardavi-Horvath, Microwave applications of soft ferrites, J. Magn. Magn. Mater. 215-216 (2000) 171-183.

[8] R. Topkaya, A. Baykal, A. Demir, Yafet–Kittel-type magnetic order in Zn-substituted cobalt ferrite nanoparticles with uniaxial anisotropy, Journal of Nanoparticle Research, 15 (2013) 1-18.

[9] S.N. Kane, M. Satalkar, Correlation between magnetic properties and cationic distribution of $Zn_{0.85-x}Ni_xMg_{0.05}Cu_{0.1}Fe_2O_4$ nano spinel ferrite: effect of Ni doping, J. Mater. Sci. 52 (2017) 3467-3477.

[10] P. Roy, J. Bera, Effect of Mg substitution on electromagnetic properties of $(Ni_{0.25}Cu_{0.20}Zn_{0.55})Fe_2O_4$ ferrite prepared by auto combustion method, J. Magn. Magn. Mater. 298 (2006) 38–42.

[11] M.H. Rashid, A.K.M. Akther Hossain, Structural, morphological and electromagnetic properties of Sc^{3+} doped Ni-Cu-Zn ferrites, Results in Physics, 11 (2018) 888-895.

[12] M.M. Eltabey, K.M. El-Shokrofy, S.A. Gharbia, Enhancement of the magnetic properties of Ni–Cu–Zn ferrites by the non-magnetic Al^{3+}-ions substitution, J. Alloys Compd. 509 (2011) 2473-2477.

[13] V. Chaudhari, S.E. Shirsath, M. Mane, R. Kadam, S. Shelke, D. Mane, Crystallographic, magnetic and electrical properties of $Ni_{0.5}Cu_{0.25}Zn_{0.25}La_xFe_{2-x}O_4$ nanoparticles fabricated by sol–gel method, J. Alloys Compd. 549 (2013) 213-220.

[14] H. Harzali, A. Marzouki, F. Saida, A. Megriche, A. Mgaidi, Structural, magnetic and optical properties of nanosized $Ni_{0.4}Cu_{0.2}Zn_{0.4}R_{0.05}Fe_{1.95}O_4$ (R = Eu^{3+}, Sm^{3+}, Gd^{3+} and Pr^{3+}) ferrites synthesized by co-precipitation method with ultrasound irradiation, J. Magn. Magn. Mater. 460 (2018) 89-94.

[15] M.A. Almessiere, Y. Slimani, A.D. Korkmaz, S. Guner, M. Sertkol, Sagar E. Shirsath, A. Baykal, Structural, optical and magnetic properties of Tm3+ substituted cobalt spinel ferrites synthesized via sonochemical approach, Ultrason Sonochem. (2019) 54: 1-10.

[16] Muhiran Abdullah Almessiere, Yassine Slimani, Abdulhadi Baykal (2019) Synthesis and characterization of $Co_{1-2x}Ni_xMn_xCe_yFe_{2-y}O_4$ nanoparticles, J. Rare Earth https://doi.org/10.1016/j.jre.2019.07.005.

[17] F. Gozuak, Y. Koseoglu, A. Baykal, H. Kavas, Synthesis and characterization of $Co_xZn_{1-x}Fe_2O_4$ magnetic nanoparticles via a PEG-assisted route, J. Magn. Magn. Mater. 321 (2009) 2170–2177

[18] Majid Niaz Akhtar, M. Babar, Sabih Qamar, Zia ur Rehman, Muhammad Azhar Khan, Structural Rietveld refinement and magnetic features of prosademium (Pr) doped Cu nanocrystalline spinel ferrites, Cer. Int. 45 (2019) 10187–10195.

[19] V.S. Kumbhar, A.D. Jagadale, N.M. Shinde, C.D. Lokhande, Chemical synthesis of spinel cobalt ferrite ($CoFe_2O_4$) nano-flakes for super-capacitor application, Appl. Surf. Sci. 259 (2012) 39-43.

[20] W. Hu, N. Qin, G. Wu, Y. Lin, S. Li, D. Bao, Opportunity of Spinel Ferrite Materials in Nonvolatile Memory Device Applications Based on Their Resistive Switching Performances, J. Am. Chem. Soc.134(36) (2012) 14658-14661.

[21] M. Pardavi-Horvath, Microwave applications of soft ferrites, J. Mag. Magn. Mat. 215–216 (2000) 171-183.

[22] N. Nücker, J. Fink, J. C. Fuggle, P. J. Durham, and W. M. Temmerman, Evidence for holes on oxygen sites in the high- Tc superconductors $La_{2-x}Sr_xCuO_4$ and YBa_2Cu3O_{7-y}, Phys. Rev. B. 37 (1988) 5158-

[23] H. L. Ju, H.-C. Sohn, and Kannan M. Krishnan, Evidence for O2p Hole-Driven Conductivity in La1−xSrxMnO3 (0≤x≤0.7) and La0.7Sr0.3MnOz Thin Film, Phys. Rev. Lett. 79, (1997) 3230-

[24] G.D.Tang, Z.Z.Li, L.Ma, W.H.Qi, L.Q.Wu, X.S.Ge, G.H.Wu, F.X.Hu "Three models of magnetic ordering in typical magnetic materials" Physics Reports. 758 (2018) 1-

[25] J. J. Qian, W. H. Qi, Z. Z. Li, L. Ma, G. D. Tang, Y. N. Du, M. Y. Chen, G. H. Wu and F. X. Hu "Spin-dependent and spin-independent channels of electrical transport in perovskite manganites" RSC Advances, 8 (2018) 4417-

[26] B. Unal, İ.S. Ünver, H. Güngüneş, U. Topal, A. Baykal, Hüseyin Sözeri, Microwave, dielectric and magnetic properties of Mg-Ti substituted NiZn-ferrite nanoparticles, Cer. Int. 42 (2016) 17317-17331.

[27] N.H. Alonizan and R. Qindeel, Structural and magnetic properties of ytterbium substituted spinel ferrites, Appl. Phys. A 124 (2018) 408.

[28] S. Ukishima, M. Iijima, M. Sato, Y. Takahashi, E. Fukada, Heat resistant polyimide films with low dielectric constant by vapor deposition polymerization, Thin Solid Films 308–309 (1997) 475-479.

[29] J. C. Maxwell, A Treatise on Electricity and Magnetism, Oxford University Press, Oxford, 1873.

[30] K.W. Wagner, Zur Theorie der Unvollkommenen Dielektrika, Annalen der Physik, 40 (1913) 817-855.

[31] C.G. Koops, On the Dispersion of Resistivity and Dielectric Constant of Some Semiconductors at Audiofrequencies, Physical Review 83 (1) (1951) 121- 124.

[32] K.M. Batoo, S. Kumar, C.G. Lee, Study of dielectric and ac impedance properties of Ti doped Mn ferrites, Current Applied Physics 9(6) (2009) 1397-1406.

[33] J S. Ghodake, R.C. Kambale, S.V. Salvi, S.R. Sawant, S. S. Suryavanshi, "Electric properties of Co substituted Ni–Zn ferrites", J. Alloys Compd. (1–2) (2009) 830-834.

[34] W. Qu, T.M. Ko, R.H. Vora, T.S Chung, Effect of polyimides with different ratios of para- to meta-analogous fluorinated diamines on relaxation process, Polymer 42(15) (2001) 6393-6401.

[35] B. Unal, Z. Durmus, H. Kavas, A. Baykal, M.S. Toprak, Synthesis, conductivity and dielectric characterization of salicylic acid–Fe_3O_4 nanocomposite, Mater. Chem. Phys. 123(1) (2010) 184-190.

[36] J. Coey, J.M.D. Noncollinear spin arrangement in ultrafine ferromagnetic crystallites, Physical Review Letters 27(17) (1971) 1140-1142.

[37] D. Değer, K. Ulutas, Conduction and dielectric polarization in Se thin films, Vacuum 72(3) (2003) 307-312.

[38] D.J. Griffiths, "Introduction to Electrodynamics", 3rd ed., Prentice Hall, 1998 ISBN:0-13-805326-X.

[39] B. Unal, M.S. Toprak, Z. Durmuş, H. Sözeri, A. Baykal, Synthesis, structural and conductivity characterization of alginic acid-Fe_3O_4 nanocomposite, J. Nanopart. Res. 12(2010) 3039.

List of Figures

Figure 1. XRD patterns of $Ni_{0.4}Cu_{0.2}Zn_{0.4}La_xY_xFe_{2-x}O_4$ (x=0.00-0.10) NSFs.

Figure 2. SEM images of the selected $Ni_{0.4}Cu_{0.2}Zn_{0.4}La_xY_xFe_{2-x}O_4$ NSFs with x=0.00, 0.02, 0.06 and 0.10 NSFs

Figure 3. EDX spectra and elemental mapping of $Ni_{0.4}Cu_{0.2}Zn_{0.4}La_xY_xFe_{2-x}O_4$ (x=0.04 and 0.08) NSFs.

Figure 4. FT-IR spectra of $Ni_{0.4}Cu_{0.2}Zn_{0.4}La_xY_xFe_{2-x}O_4$ (x=0.00-0.10) NSFs.

Figure 5. 3D representation of ac conductivity of $Ni_{0.4}Cu_{0.2}Zn_{0.4}La_xY_xFe_{2-x}O_4$ NSFs for a variety of La^{3+} and Y^{3+} ions co-substitutional ratios of x=0.00 - 0.10.

Figure 6. Arrhenius plot of dc conductivity for various co-substitutional ratios of La^{3+} and Y^{3+} ions in $Ni_{0.3}Cu_{0.3}Zn_{0.4}Fe_2O_4$ NSFs.

Figure 7. The 3D representations of dielectric constant of $Ni_{0.4}Cu_{0.2}Zn_{0.4}La_xY_xFe_{2-x}O_4$ NSFs for a variety of La^{3+} and Y^{3+} ions co-substitutional ratios of x=0.00 - 0.10.

Figure 8. The 3D representations of dielectric loss of $Ni_{0.4}Cu_{0.2}Zn_{0.4}La_xY_xFe_{2-x}O_4$ NSFs for a variety of La^{3+} and Y^{3+} ions co-substitutional ratios of x=0.00 - 0.10.

Figure 9. The 3D representations of dielectric tangent loss of $Ni_{0.4}Cu_{0.2}Zn_{0.4}La_xY_xFe_{2-x}O_4$ NSFs for a variety of La^{3+} and Y^{3+} ions co-substitutional ratios of x=0.00 - 0.10.

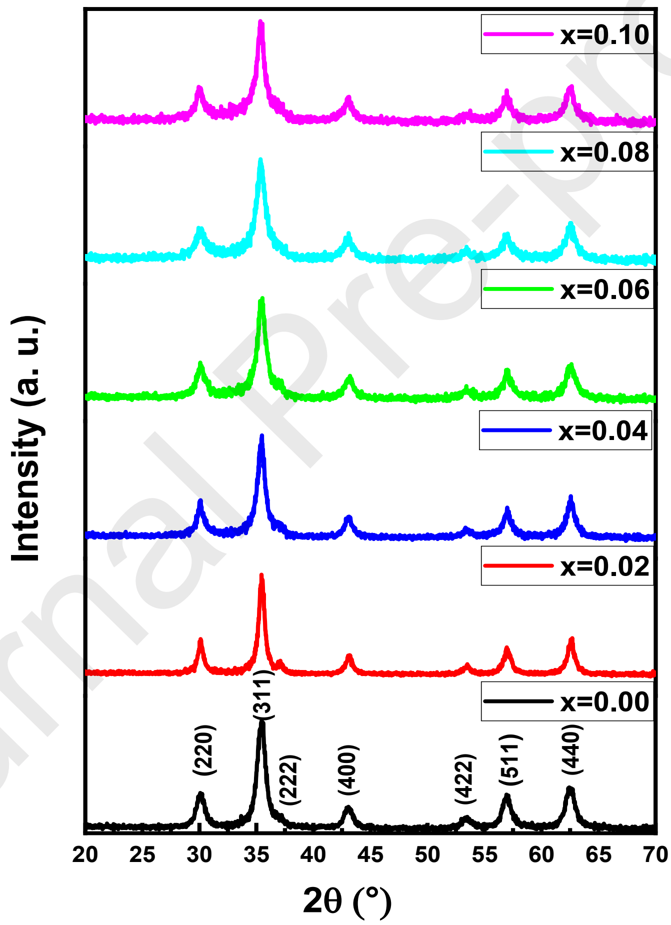

Figure 1.

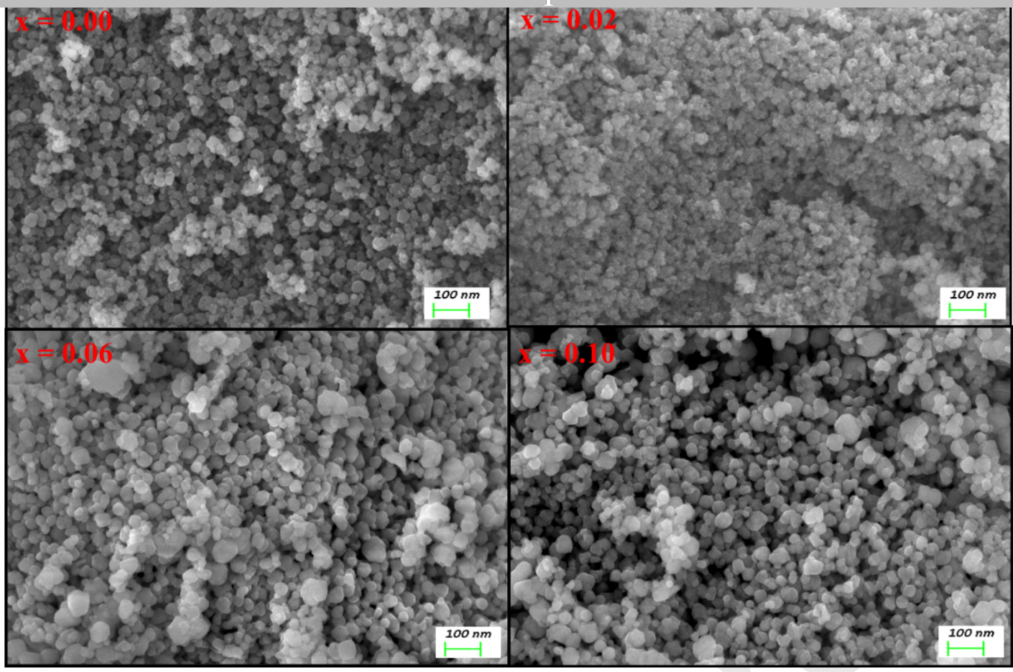

Figure 2.

x = 0.04

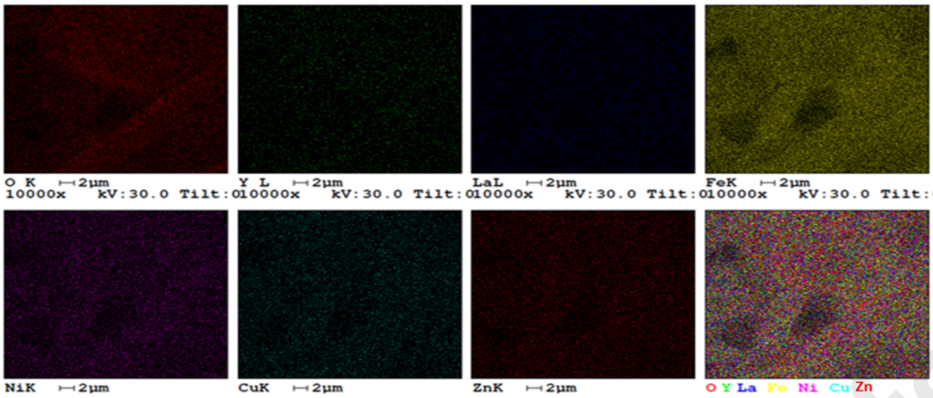

Elements	Weight % (Exp.)	Weight %(Theo.)
Ni	9.71	11.14
Cu	4.93	8.03
Zn	11.32	12.4
Fe	45.31	50.8
La	2.97	2.63
Y	1.46	1.7
O	24.3	15.19

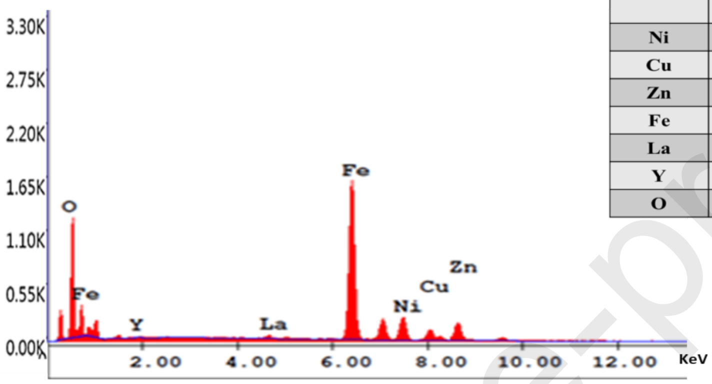

x = 0.08

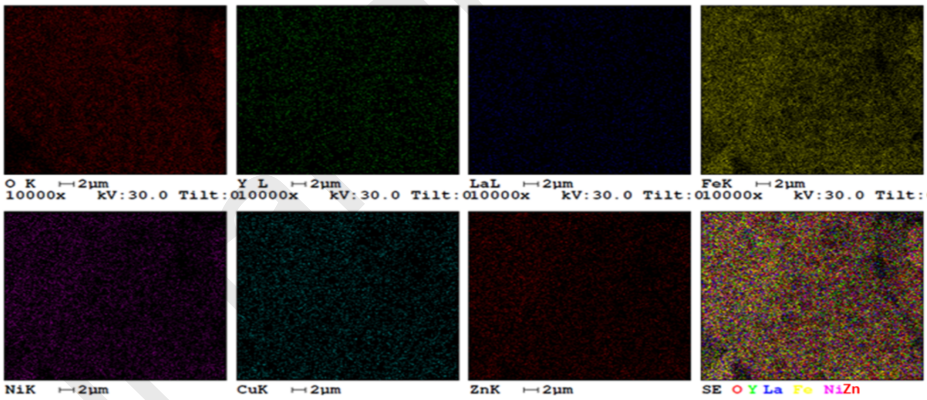

Elements	Weight % (Exp.)	Weight %(Theo.)
Ni	9.83	10.87
Cu	4.57	5.9
Zn	11.09	12.1
Fe	43.48	47.7
La	4.58	5.16
Y	3.21	3.31
O	23.24	14.86

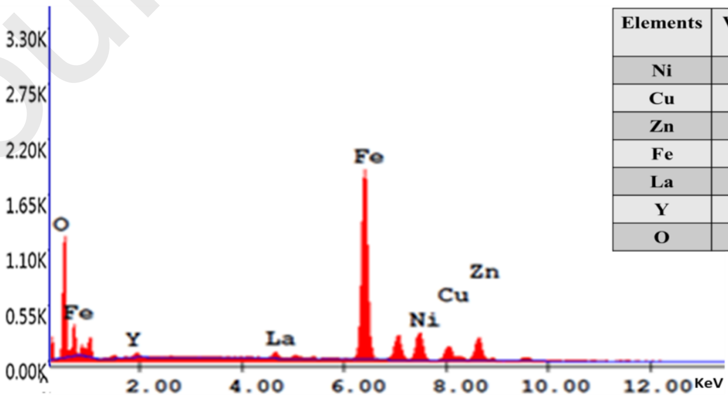

Figure 3.

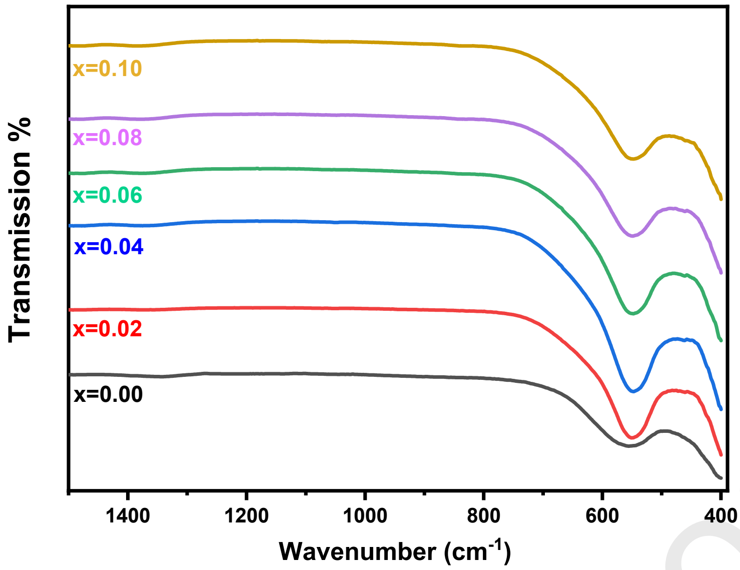
x=0.10
x=0.08
x=0.06
x=0.04
x=0.02
x=0.00
Transmission %
1400
1200
1000
800
600
400
Wavenumber (cm-1)

Figure 4.

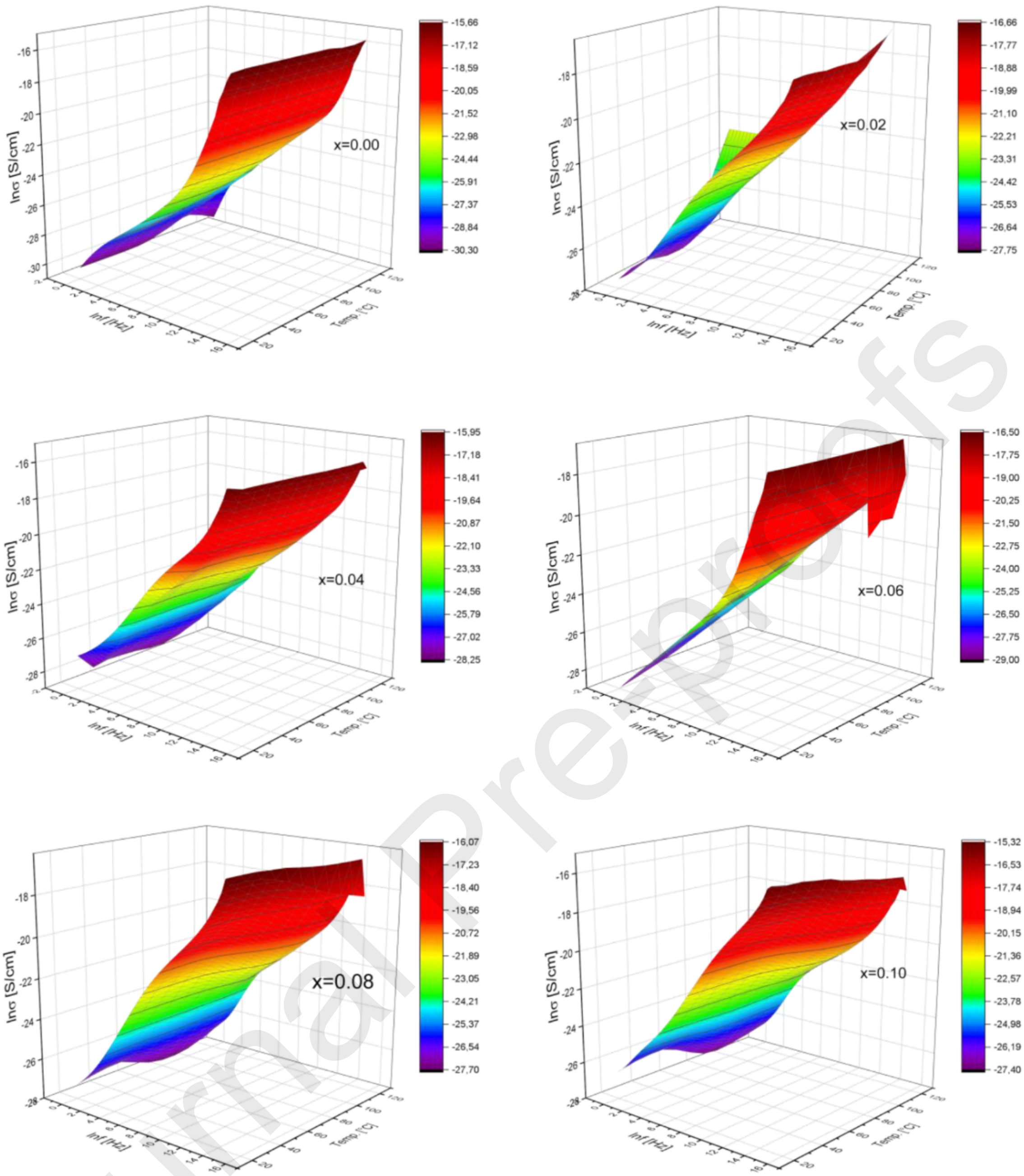

Figure 5.

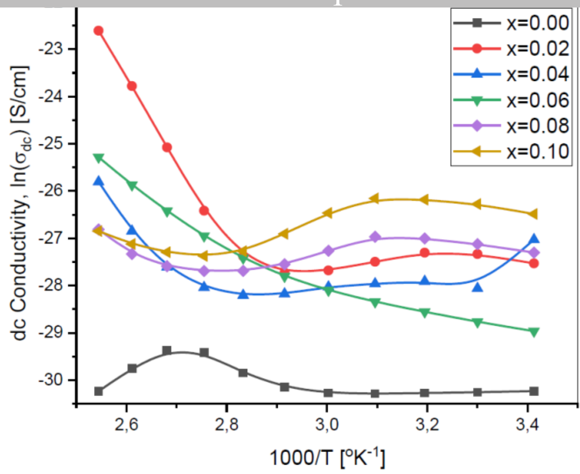
dc Conductivity, ln(σdc) [S/cm]
-23
-24
-25
-26
-27
-28
-29
-30
2,6
2,8
3,0
3,2
3,4
1000/T [°K-1]
x=0.00
x=0.02
x=0.04
x=0.06
x=0.08
x=0.10

Figure 6.

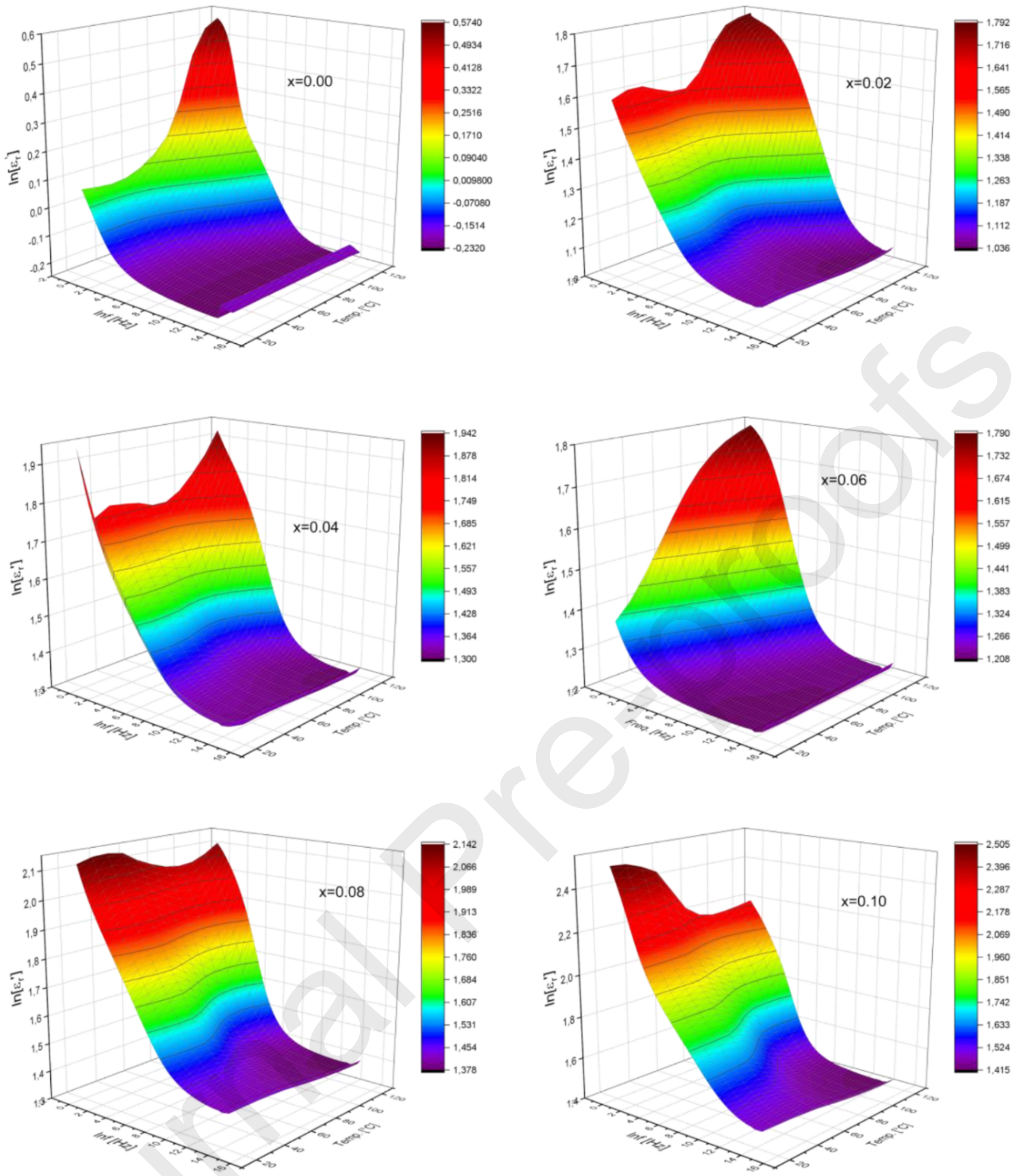

Figure 7.

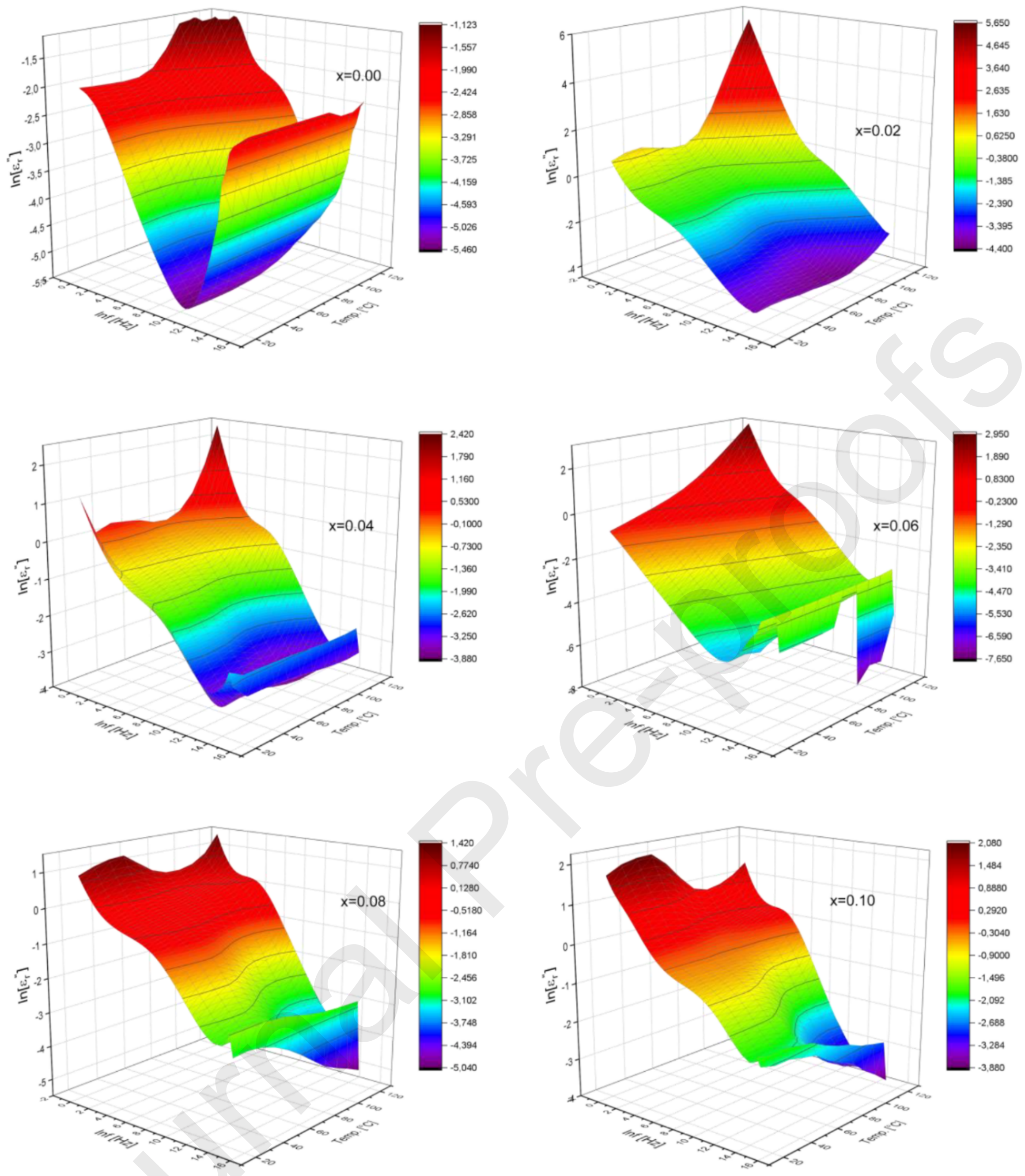

Figure 8.

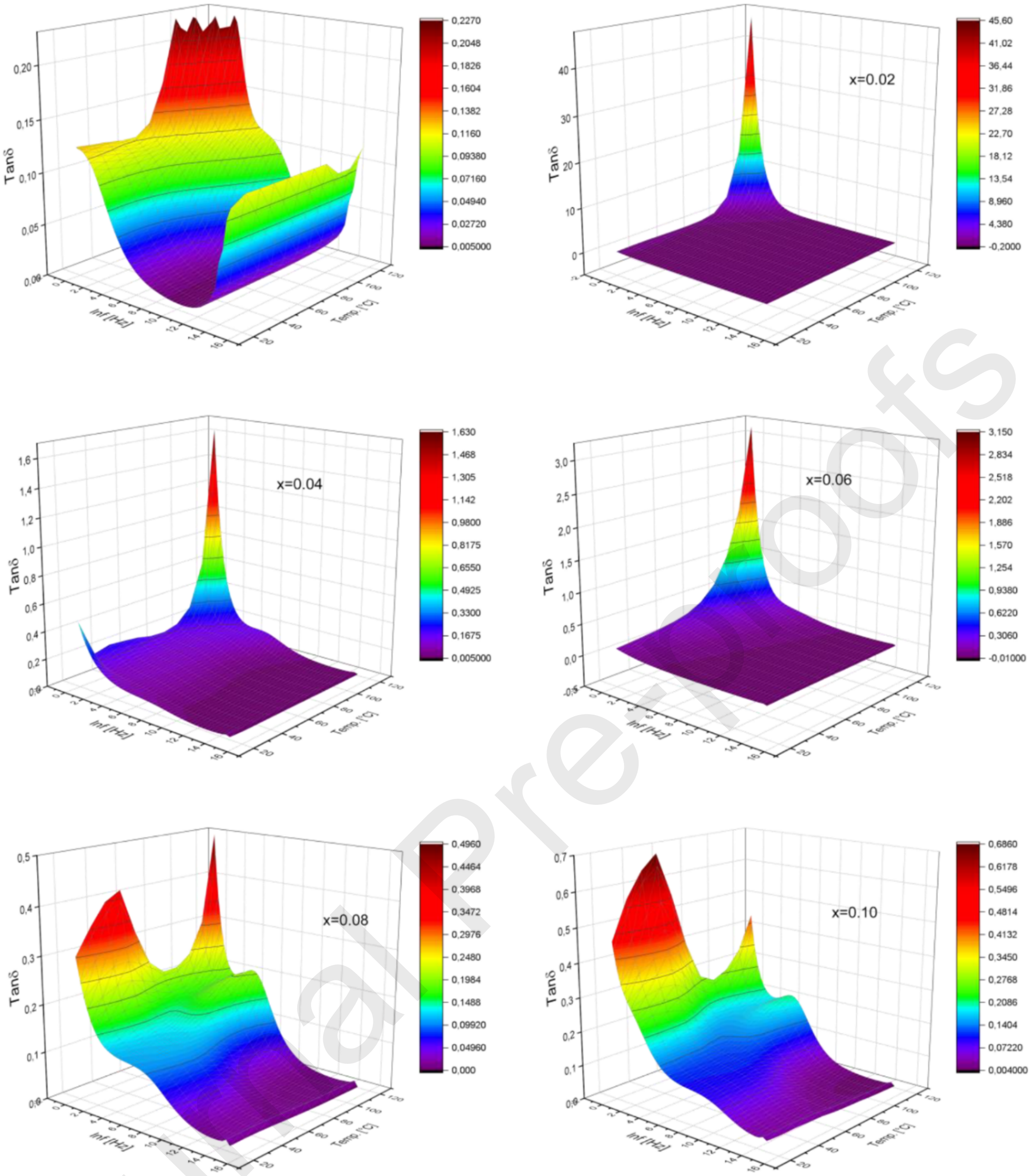

Figure 9.

List of Tables

Table 1. Refined structural parameters for $Ni_{0.4}Cu_{0.2}Zn_{0.4}La_xY_xFe_{2-x}O_4$ (x=0.00 – 0.10) NSFs

x	a(Å)	V(Å)^3	D_{XRD} (nm) ±0.04	χ^2(chi^2)	R_{Bragg}
0.00	8.397(4)	592.14	22.8	1.36	2.73
0.02	8.398(5)	592.39	21.6	1.78	1.90
0.04	8.406(7)	594.12	20.6	1.56	5.96
0.06	8.408(6)	594.52	17.3	1.47	5.36
0.08	8.410(4)	594.90	16.8	1.24	5.17
0.10	8.416(0)	596.09	12.4	1.25	2.41

Research Highlights

- La–Y substituted Ni-Cu-Zn nanospinel ferrites (NSFs) which have been synthesized via ultrasonic approach.
- The impedance spectrocopy technique was used for the analysis of electrical and dielectric properties of La^{3+} and Y^{3+} ions co-substituted $Ni_{0.3}Cu_{0.3}Zn_{0.4}Fe_2O_4$ NSFs.
- Electrical and dielectric properties shows that **(i)** ac conductivity obeys the power exponent rules; **(ii)** the activation energies for the $Ni_{0.3}Cu_{0.3}Zn_{0.4}Fe_2O_4$ NPs fluctuate with the co-substitution ratios of La^{3+} and Y^{3+} ions; **(iii)** both dielectric loss and dielectric constant decrease sharply with increasing frequencies under a power law formalism.

Author Statement

Synthesis of the sample, writing—original draft preparation, investigation dielectric properties and writing, investigation, Supervision, review and editing;

participated in drafting the article or revising it critically for important intellectual content; gave final approval of the version to be submitted and any revised version; participated sufficiently in the work to take public responsibility for appropriate portions of the content.

(1). Synthesis of the sample, writing—original draft preparation, Munirah Abdullah Almessiere;

(2). Investigation dielectric properties and writing, B. Ünal , Y. Slimani

(3). Supervision, Abdulhadi Baykal and I. Ercan

(4). Review and Editing, Y. Slimani, A.D. Korkmaz

Conflict Of Interest Statement:

The authors M. Almessiere, B. Ünal, Y. Slimani, A.D. Korkmaz, A. Baykal and I. Ercan have no conflict of interest.